A Finite-Element Procedure Based on a Boundary-Value Approach for the Evaluation of the Electromagnetic Exposure in Biological Phantoms

Salvatore Caorsi, *Member, IEEE*, Emanuela Bermani, and Andrea Massa, *Member, IEEE*

***Abstract*—In this paper, a finite-element method, based on a boundary-value approach, for the evaluation of the electric-field distribution in exposed biological phantoms is presented. Starting from the measurement of the electric field around the phantom, the field prediction is obtained by solving a boundary-value problem. This allows to avoid the description of the electromagnetic source and to estimate of the electric-field distribution also when the illuminating source is unknown or when its numerical model is not available. In order to show the effectiveness of the proposed approach, some numerical results, concerning a two-dimensional geometry, are provided. Firstly, the accuracy and validity of the electromagnetic prediction are assessed by comparing numerical with reference solutions (analytically computed). In order to demonstrate the efficiency, robustness, and capability of this technique, different measurement strategies, noisy environments, and errors in the data acquisition are then taken into account.**

***Index Terms*—Bioelectromagnetics, boundary-value approach, electromagnetic interactions, finite-element method.**

I. Introduction

In response to continued and growing public concerns on possible adverse health effects of electric, magnetic, and electromagnetic fields, many research activities have been carried out over the last years. Earlier studies were mainly focused upon extremely low frequency (ELF) [1]–[3] in public environments, such as high-voltages lines and household appliances, and in occupational environments. However, because of the rapid development and deployment of mobile and wireless communications, the focus has recently been largely shifted toward higher frequencies. Several direct approaches have been developed to evaluate the electromagnetic exposure to RF and microwave frequencies. Analytic solutions [4]–[6], as well as numerical techniques, such as the method of moment [7], the finite-element method [8], [9], some hybrid methods [10]–[12] and, in particular, the finite-difference method [13]–[17] have been taken into account. These approaches allow to obtain a good accuracy in the estimation of the electromagnetic-field distribution in a given phantom when an accurate model of the radiating source is available.

Manuscript received August 10, 2001; revised November 29, 2001.

S. Caorsi is with the Department of Electronics, University of Pavia, I-27100 Pavia, Italy (e-mail: s.caorsi@ele.unipv.it).

E. Bermani and A. Massa are with the Department of Information and Communication Technology, University of Trento, I-38050 Trento, Italy (e-mail: emanuela.bermani@ing.unitn.it; andrea.massa@ing.unitn.it).

Digital Object Identifier 10.1109/TMTT.2002.803423.

However, in some situations, a numerical description of the illuminating source could be difficult and, in other cases (for instance, if the electromagnetic source is completely unknown) even impossible. In these situations, the evaluation of the electromagnetic field could be a challenging problem. It has been shown [18]–[22] that different electromagnetic sources (i.e., electromagnetic sources differing in shape, position, radiation pattern, etc.), as well as the choice of a specific numerical model of the illumination source, produce not negligible variations in the electromagnetic-field distribution induced in a fixed biological structure.

For this reason, numerical approaches, avoiding the numerical modeling of the illumination source, results certainly very attractive in these situations.

Recently, Caorsi and Massa [23], [24] faced the problem by considering an *inverse* approach based on a microwave imaging technique. The method allows to predict the electric-field distribution in a given biological structure through the minimization of a suitably defined cost function. The numerical modeling of the electromagnetic source is avoided by employing the complex [24] or amplitude-only [25] values of the scattered electric field, measured around the phantom, and those of the incident field, collected in the investigation domain.

In this paper, an alternative solution based on a *direct* approach is presented. The proposed approach evaluates the induced electromagnetic field beginning from the knowledge of the tangential component of the electric field around the biological phantom and solving a direct electromagnetic problem. By choosing a proper numerical domain and by considering the measurement data as boundary conditions, the problem is formulated in terms of a boundary-value problem. No description of the illuminating source is required. The electromagnetic source is completely described by means of the values of the tangential component of the total electric field measured on the boundary.

In the following, the proposed technique is illustrated and deeply assessed. The dependence of the accuracy in the field prediction on the number of measurement points and the robustness of the approach to noisy input data are checked by means of selected numerical examples. Furthermore, the presence of possible errors in the positioning of the data acquisition system is taken into account.

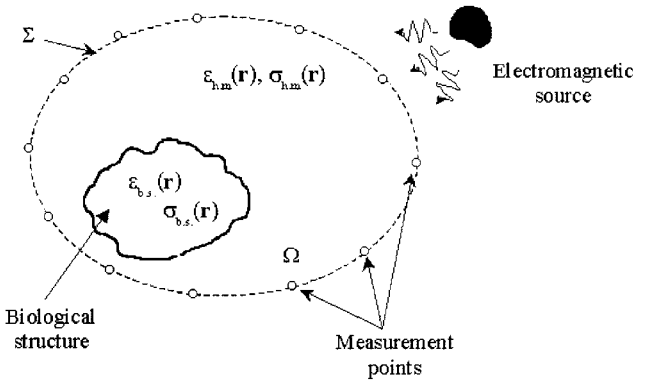

Fig. 1. Problem geometry.

II. Mathematical Formulation

Let us consider the geometry shown in Fig. 1. An electromagnetic source illuminates a biological structure characterized by a known dielectric permittivity $\varepsilon_{\mathrm{b.s.}}(\mathbf{r})$ and an electric conductivity $\sigma_{\mathrm{b.s.}}(\mathbf{r})$. The object is located inside a host medium whose dielectric parameters are $\varepsilon_{\mathrm{h.m.}}(\mathbf{r})$ and $\sigma_{\mathrm{h.m.}}(\mathbf{r})$. The magnetic permeability is everywhere as that of the free space. Let Σ be a closed surface defining a region Ω (investigation region) to which the biological structure belongs. Moreover, let the illumination source be external to the investigation region.

Starting from the knowledge of the tangential component of the electric field on Σ, the evaluation of the electric-field distribution inside the biological structure can be formulated as a boundary value problem

$$\begin{cases} \nabla \times \nabla \times \mathbf{E}(\mathbf{r}) - \omega^2 \varepsilon(\mathbf{r}) \mu_o \mathbf{E}(\mathbf{r}) = 0, & \text{in } \Omega \\ \mathbf{n} \times \mathbf{E}(\mathbf{r}) = \mathbf{g}(\mathbf{r}), & \text{on } \Sigma \end{cases} \tag{1}$$

where $\mathbf{n}$ indicates the outward normal vector on Σ, $\varepsilon(\mathbf{r})$ is the complex dielectric permittivity, and $\mathbf{g}(\mathbf{r})$ is a given vectorial function defined on Σ.

The problem in (1) is well posed. Moreover, the illuminating source is completely described by means of boundary conditions (i.e., the value of the tangential component of $\mathbf{E}(\mathbf{r})$ on Σ). This allows to obtain the distribution of the electric field inside the whole biological structure as the unique solution of (1) without requiring any modeling of the electromagnetic source [26].

In order to numerically solve (1), a finite-element approach is considered. By assuming two different weighting functions $\mathbf{w}$ and $\overline{\mathbf{w}}$, a variational formulation of (1) is firstly obtained as follows:

$$\int_\Omega \left[\nabla \times \mathbf{E}(\mathbf{r}) \cdot \nabla \times \mathbf{w}(\mathbf{r}) - \omega^2 \varepsilon(\mathbf{r}) \mu_o \mathbf{E}(\mathbf{r}) \cdot \mathbf{w}(\mathbf{r})\right] d\Omega = \int_\Sigma \left[\mathbf{n} \times \nabla \times \mathbf{E}(\mathbf{r})\right] \cdot \mathbf{w}(\mathbf{r})\, d\Sigma + \int_\Sigma \left[\mathbf{n} \times \mathbf{E}(\mathbf{r}) - \mathbf{g}(\mathbf{r})\right] \cdot \overline{\mathbf{w}}(\mathbf{r})\, d\Sigma. \tag{2}$$

By choosing the weighting function $\mathbf{w}(\mathbf{r})$ so that it vanishes on Σ and by imposing that the electric-field distribution $\mathbf{E}(\mathbf{r})$ satisfies the weighted boundary condition on Σ for each $\overline{\mathbf{w}}(\mathbf{r})$, (2) can be rewritten as

$$\int_\Omega \left[\nabla \times \mathbf{E}(\mathbf{r}) \cdot \nabla \times \mathbf{w}(\mathbf{r}) - \omega^2 \varepsilon(\mathbf{r}) \mu_o \mathbf{E}(\mathbf{r}) \cdot \mathbf{w}(\mathbf{r})\right] d\Omega = 0. \tag{3}$$

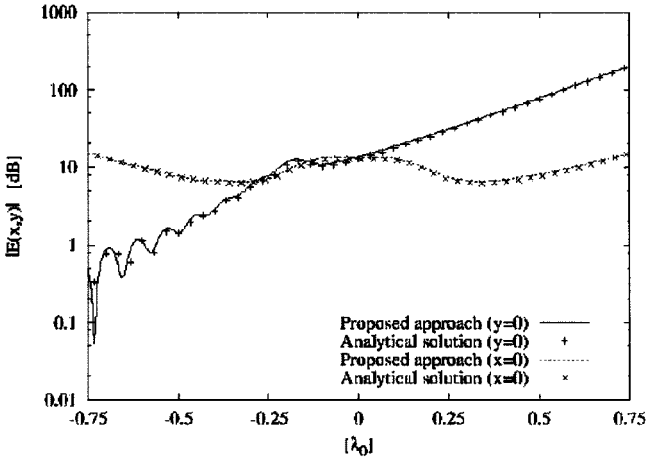

(a)

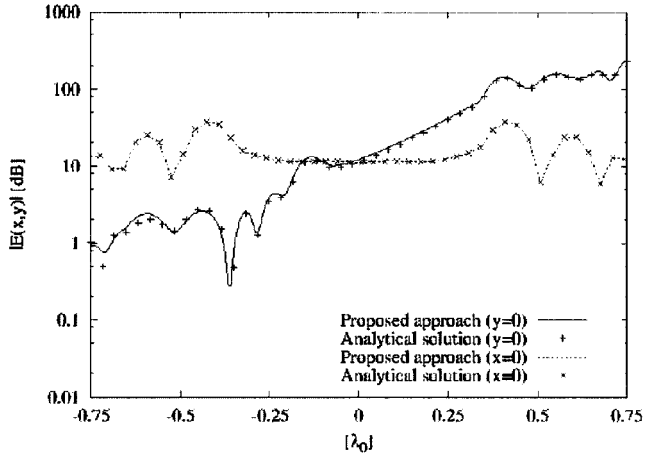

(b)

Fig. 2. Amplitude of the electric field along the x- and y-axis. (a) Homogeneous cylinder. (b) Multilayer cylinder.

A finite-element space discretization of (3) is then obtained by introducing a triangulation τ_h of $\overline{\Omega}$ (where $\overline{\Omega} = \Omega \cup \Sigma$) and by defining a specific finite-element basis $V = \{\mathbf{v}_i(\mathbf{r}), i = 1, \ldots, m\}$ on τ_h, which spans a finite dimensional subspace $V_h \in H(\mathrm{curl}; \Omega)$ (where $H(\mathrm{curl}; \Omega) = \{\mathbf{w}(\mathbf{r})$: $\int_\Omega |\mathbf{w}(\mathbf{r})|^2\, d\Omega < +\infty$, $\int_\Omega |\nabla \times \mathbf{w}(\mathbf{r})|^2\, d\Omega < +\infty\}$ being h, the maximum diameter of the elements of the triangulation τ_h).

Let us express $\mathbf{E}(r)$ as a linear combination of the finite-element basis

$$\mathbf{E}(\mathbf{r}) = \sum_{i=1}^{m} e_i \mathbf{v}_i(\mathbf{r}). \tag{4}$$

By imposing that (3) holds for each $\mathbf{w}_j(r) \in W$, where $W = \{\mathbf{w}_j(\mathbf{r}), j = 1, \ldots, k$: $\mathbf{w}_j(\mathbf{r}) \in V_h$, $\mathbf{w}_j(\mathbf{r}) = 0$ on $\Sigma\}$, the following system is obtained:

$$\sum_{i=1}^{m} \int_\Omega e_i \left[\nabla \times \mathbf{v}_i(\mathbf{r}) \cdot \nabla \times \mathbf{w}_j(\mathbf{r}) - \omega^2 \varepsilon(\mathbf{r}) \mu_o e_i \mathbf{v}_i(\mathbf{r}) \cdot \mathbf{w}_j(\mathbf{r})\right] d\Omega = 0 \qquad \forall\, \mathbf{w}_j(\mathbf{r}) \in W. \tag{5}$$

In a matrix form, it can be rewritten as

$$\left[\mathbf{S}_{jf} - \omega^2 \mu_o \mathbf{T}_{jf}\right] \mathbf{e}_f = -\left[\mathbf{S}_{jp} - \omega^2 \mu_o \mathbf{T}_{jp}\right] \mathbf{e}_p \tag{6}$$

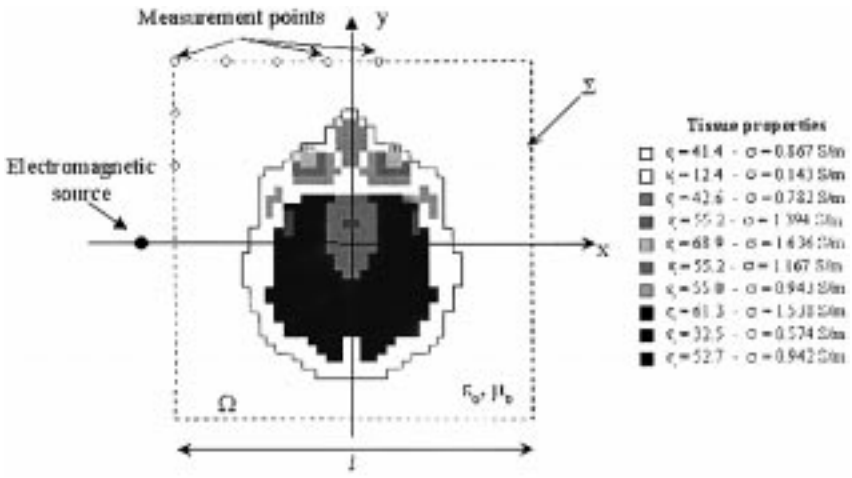

Fig. 3. Model of the biological phantom.

where $\mathbf{e}_f$ and $\mathbf{e}_p$ are the array of the unknown coefficients and the array of known boundary coefficients, respectively; the matrix elements $S_{j,i}$ and $T_{j,i}$ are defined as

$$S_{j,i} = \int_{\Omega} \nabla \times \mathbf{v}_i(\mathbf{r}) \cdot \nabla \times \mathbf{w}_j(\mathbf{r})\, d\Omega \tag{7}$$

$$T_{j,i} = \int_{\Omega} \varepsilon(\mathbf{r}) \mathbf{v}_i(\mathbf{r}) \cdot \mathbf{w}_j(\mathbf{r})\, d\Omega \tag{8}$$

where $\mathbf{v}_f(\mathbf{r})$, $\mathbf{v}_p(\mathbf{r}) \in V$ verify $\mathbf{v}_f(\mathbf{r}) = 0$ and $\mathbf{v}_p(\mathbf{r}) \neq 0$ on Σ, respectively.

Since the linear algebraic system (6) is well conditioned [27], the solution can be obtained by means of a standard numerical technique [28]. As far as basis and test functions are concerned ($\mathbf{v}_i$; $i = 1, \ldots, m$ and $\mathbf{w}_j$; $j = 1, \ldots, k$, respectively), edge elements [29] are generally used when vectorial problems are addressed. Nonetheless, linear Lagrange basis functions [27] can be considered when scalar formulation are handled.

III. Numerical Results

In order to preliminary assess the effectiveness of the proposed approach, a test case, for which an analytical reference solution is available, is analyzed.

A circular cylinder, illuminated by an infinite electric line positioned $1.5\lambda_o$ far from the object (being λ_o, the wavelength in free space), is considered. The axis of the cylinder is coincident with the z-axis and its radius is equal to $0.75\lambda_o$. The investigation domain is a square region $l = 2.4\lambda_o$ in side, noncoaxial with the dielectric cylinder, and Σ is its boundary. In order to discretize $\overline{\Omega}$, a triangular mesh is obtained starting from an uniform grid with square elements $\Delta_b = 0.0125\lambda_o$ sided. Basis functions are Lagrangian elements [27]. The values of the tangential component of $\mathbf{E}(\mathbf{r})$ are analytically computed at M measurement points coincident with all the boundary nodes on Σ.

Fig. 2(a) and (b) shows the amplitude of the electric field, along both the x- and y-axis, for a homogeneous ($\varepsilon_r = 40.0$ and $\sigma = 0.5$ S/m) and for a stratified dielectric cylinder (inner layer: $\varepsilon_{r1} = 55.0$, $\sigma_1 = 0.9$ S/m,; medium layer: $\varepsilon_{r2} = 12.0$, $\sigma_2 = 0.1$ S/m, external layer $\varepsilon_{r3} = 41.0$, $\sigma_3 = 0.8$ S/m), respectively. For comparison, analytical solutions are also reported. In order to quantitatively evaluate the prediction accuracy, some error figures are defined as follows:

$$\xi(x_n, y_n) = \frac{\Big|\big|\mathbf{E}_{\rm act}(x_n, y_n)\big| - \big|\mathbf{E}_{\rm pred}(x_n, y_n)\big|\Big|}{\big|\mathbf{E}_{\rm act}(x_n, y_n)\big|} \quad \forall n = 1, \ldots, N \quad \text{(amplitude error)} \tag{9}$$

$$\phi(x_n, y_n) = \frac{\Big|ph_{\rm act}\{\mathbf{E}(x_n, y_n)\} - ph_{\rm pred}\{\mathbf{E}(x_n, y_n)\}\Big|}{2\pi} \quad \forall n = 1, \ldots, N \quad \text{(phase error)} \tag{10}$$

where (x_n, y_n) indicates the position of the nth node of the mesh belonging to the biological body, N is the number of nodes inside the biological body, the subscripts act and pred indicate actual and predicted values, respectively, and $|\mathbf{E}(x, y)|$ and $ph\{\mathbf{E}(x, y)\}$ are the amplitude and the phase of the electric field, respectively.

As far as the first example is concerned, the average amplitude error $\mathrm{av}\{\xi(x, y)\}$ is equal to -87.1 dB, for the homogeneous cylinder and -85.7 dB for the stratified one. The average phase errors $\mathrm{av}\{\phi(x, y)\}$ are $2.18 \cdot 10^{-5}$ and $1.66 \cdot 10^{-5}$, respectively.

The second test case is devoted to analyze a more complex structure. A discretized version of a horizontal slice of a human head, located in the vacuum, is assumed as biological phantom (Fig. 3). In this example, Ω is a square region $l = 0.648\lambda_o$ discretized with triangular elements obtained starting from an uniform grid of square elements $\Delta_b = 0.018\lambda_o$ in size. The values of the tangential component of $\mathbf{E}(\mathbf{r})$ are collected at M measurement points uniformly distributed along Σ.

Input data are synthetically generated by considering a larger discretization domain ($l_u = 1.98\lambda_o$) with different mesh size ($\Delta_u = \Delta_b/2$), illuminated by an infinite electric line, located $0.126\lambda_o$ far from the biological structure. The computational domain is limited by means of an anisotropic perfectly matched layer [30].

Firstly, the electric-field distribution inside the biological structure is computed by considering the measurement points coincident with all the boundary nodes. Fig. 4(a) and (b) shows the amplitude and phase of the predicted field, respectively.

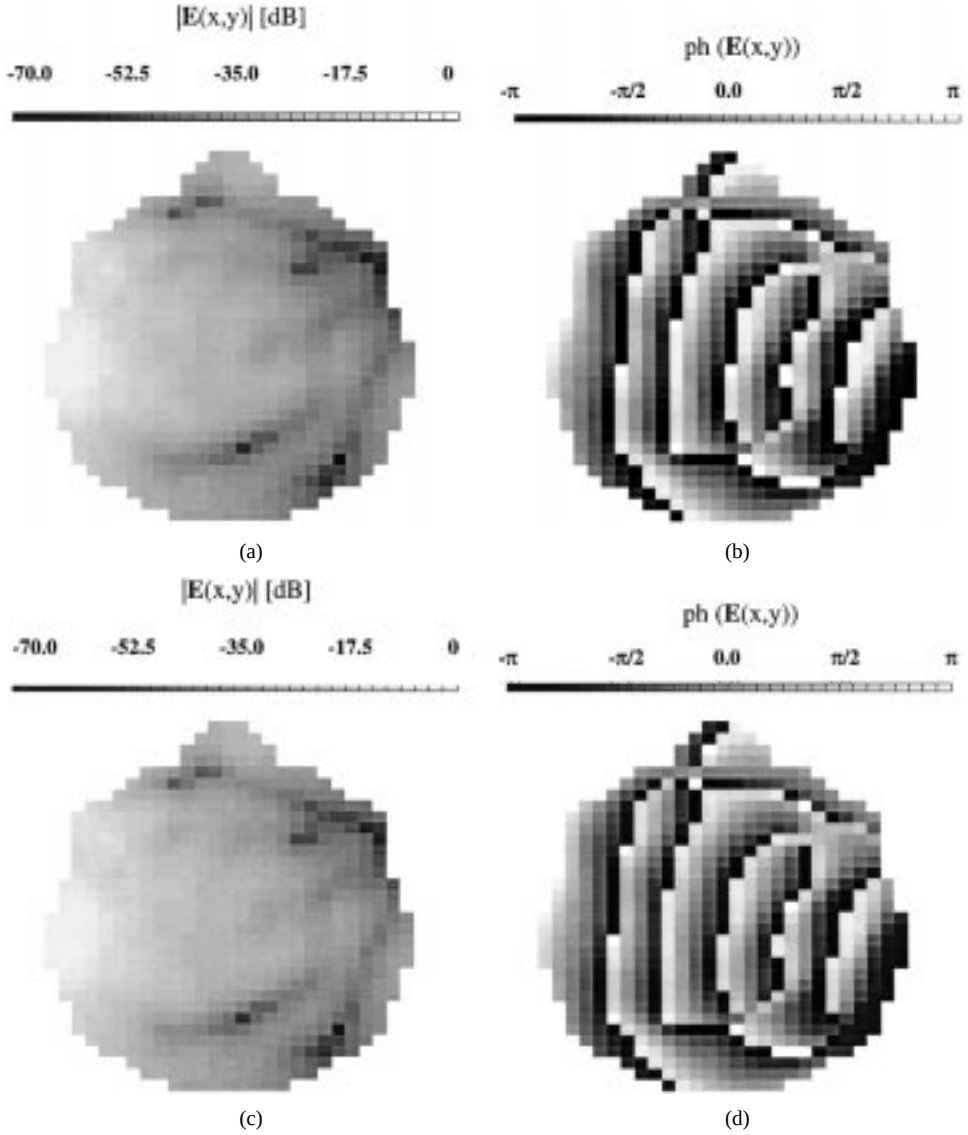

Fig. 4. Electric-field distribution. Estimated field distribution ($M = 144$). (a) Amplitude. (b) Phase. Reference distribution: (c) Amplitude. (d) Phase.

By comparing estimated distributions with the actual values [shown in Fig. 4(c) and (d)], a good agreement can be observed in the whole biological structure. The average amplitude error $\mathrm{av}\{\xi(x, y)\}$ is equal to -89.9 dB and the average phase error $\mathrm{av}\{\phi(x, y)\}$ is $2.28 \cdot 10^{-5}$. These indications clearly confirm that, if the number of measurement points is equal to that of the boundary nodes and if the measurement points are located at the boundary nodes, the field prediction results very accurate. However, since a large number of measurement points could be necessary, the measurement could be impracticable with an experimental apparatus.

In order to verify if the number of measurement point can be reduced, the dependence of the field prediction on the number of measurement points is evaluated. To this aim, M equally spaced boundary nodes are taken into account as measurement points. Their positioning, along the squared surface, has been realized locating the first measurement point at the low left-hand-side corner of the measurement surface and then proceeding with a uniform spacing in a clockwise direction. The values of the tangential component of the electric field on remaining boundary nodes are obtained by means of a quadratic interpolation of measured data.

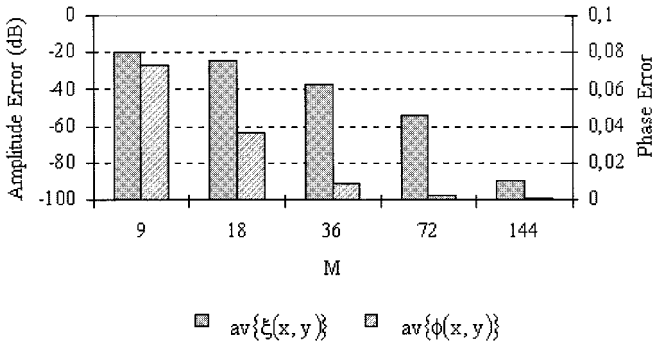

Fig. 5. Prediction quality versus M. Average errors.

Fig. 5 gives the average values of the error figures for different values of M. In particular, starting from 1/2 until 1/16 ($M = 9$) of boundary nodes have been considered. Whatever the value of M is, the amplitude of the electric field is well estimated

TABLE I
ESTIMATION OF THE PEAK AMPLITUDE (INSIDE THE BIOLOGICAL BODY) VERSUS M. AMPLITUDE ERROR

M	$\xi(x_p, y_p)$
144	-120 dB
72	-50.2 dB
36	-30.2 dB
18	-25.8 dB
9	-21.8dB

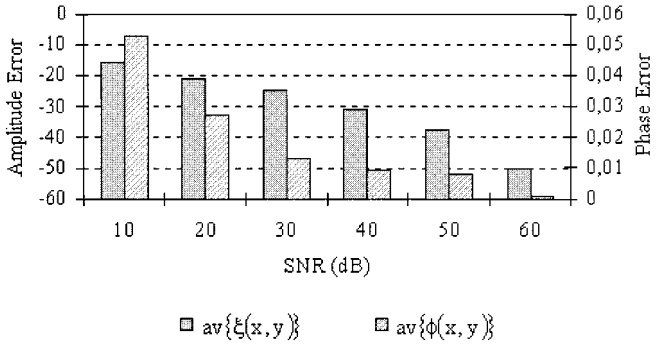

Fig. 6. Prediction quality versus SNR. Average errors.

with an average error $\mathrm{av}\{\xi(x, y)\} \leq -19.6$ dB and the phase is predicted with an average error $\mathrm{av}\{\phi(x, y)\} \leq 0.072$.

Moreover, the value of the amplitude peak (i.e., the maximum amplitude of the electric field inside the biological structure) is satisfactorily estimated (see Table I) and always the peak position (x_p, y_p) is correctly located.

In the third numerical example, the robustness of the proposed technique to noisy measurement data is investigated. In order to simulate the presence of a white Gaussian noise, a complex quantity $\zeta^{\mathrm{noise}}(\mathbf{r})$, whose real and imaginary parts are Gaussian variables characterized by zero mean value and variance depending on the fixed SNR, is added to the measurement data. For this case, input data are synthetically computed by means of the method of moments [7].

Fig. 6 shows average amplitude and phase errors for different values of the SNR. When $\mathrm{SNR} \geq 20$ dB, the average amplitude error results lower than -20.9 dB. For the range of values, the phase error is lower than 0.027. On the other hand, when the SNR further reduces, the performances of the proposed approach decrease. The electric field is no longer well estimated, in particular, at those regions where the amplitudes of the induced field are negligible with respect to the amplitude peak $(\xi(x_n, y_n) < (1/100)\xi(x_p, y_p))$.

Nevertheless, the location of the amplitude peak is correctly detected and its value estimated with an error lower than -18.7 dB when $\mathrm{SNR} = 10$ dB (Fig. 7).

Finally, the influence of an incorrect positioning of the measurement system is assessed. Numerically, this situation results in a measurement contour different from the one used to generate the input data. By a numerical point-of-view, this condition is simulated by considering, besides the original measurement points $\{(x_m, y_m), m = 1, \ldots, M\}$, M of *false* observation

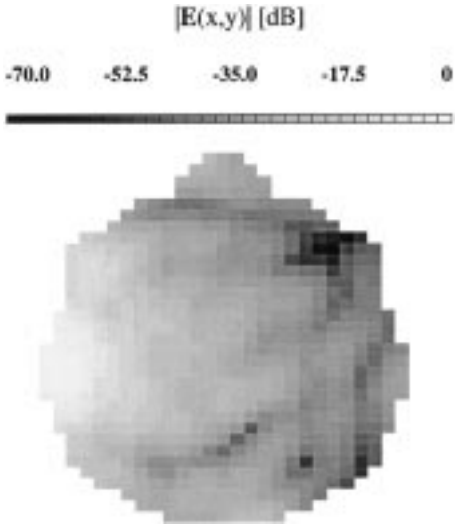

Fig. 7. Distribution of the field amplitude ($\mathrm{SNR} = 10$ dB).

TABLE II
AVERAGE AMPLITUDE ERROR ($\mathrm{av}\{\xi(x, y)\}$), AVERAGE PHASE ERROR ($\mathrm{av}\{\phi(x, y)\}$), AND ERROR IN THE PREDICTION OF THE AMPLITUDE PEAK ($\xi(x_p, y_p)$) FOR VARIOUS INCORRECT POSITIONING

t	$av\{\xi(x,y)\}$	$av\{\phi(x,y)\}$	$\xi(x_p, y_p)$
0.1	-61.0 dB	$2.77 \cdot 10^{-4}$	-55.4 dB
0.2	-54.8 dB	$5.98 \cdot 10^{-4}$	-53.2 dB
0.3	-51.6 dB	$7.62 \cdot 10^{-4}$	-51.0 dB
0.4	-51.3 dB	$1.05 \cdot 10^{-3}$	-43.7 dB
0.5	-47.3 dB	$1.22 \cdot 10^{-3}$	-42.6 dB
0.6	-43.8 dB	$1.25 \cdot 10^{-3}$	-41.8 dB
0.7	-43.9 dB	$1.65 \cdot 10^{-3}$	-41.0 dB
0.8	-43.9 dB	$1.87 \cdot 10^{-3}$	-40.7 dB
0.9	-43.1 dB	$2.93 \cdot 10^{-3}$	-39.9 dB
1.0	-40.8 dB	$2.84 \cdot 10^{-3}$	-38.0 dB

points $(\tilde{x}_m, \tilde{y}_m)$, whose position is randomly chosen so that the following condition is fulfilled:

$$(\tilde{x}_m, \tilde{y}_m) \in C_R(x_m, y_m), \qquad m = 1, \ldots, M \tag{11}$$

where $C_R(x_m, y_m)$ is a circle $R = t \cdot \nu^{\max}$ ($t \in [0 \div 1]$) in radius, centered at the mth measurement point; $\nu^{\max} = \Delta_b/2$ approximates the maximum error of the measurement system and is related to the accuracy of experimental positioning apparatus (which strongly depends on the application, but generally it is lower than a few millimeters [31]). Measured data collected at $(\tilde{x}_m, \tilde{y}_m)$ $m = 1, \ldots, M$ are then assumed as input data at (x_m, y_m) $m = 1, \ldots, M$. Table II gives error statistics for different value of the positioning parameter t.

For completeness, Fig. 8(a)–(c) gives the distributions of $\xi(x, y)$ when $t = 0.1$, $t = 0.5$, and $t = 1.0$, respectively.

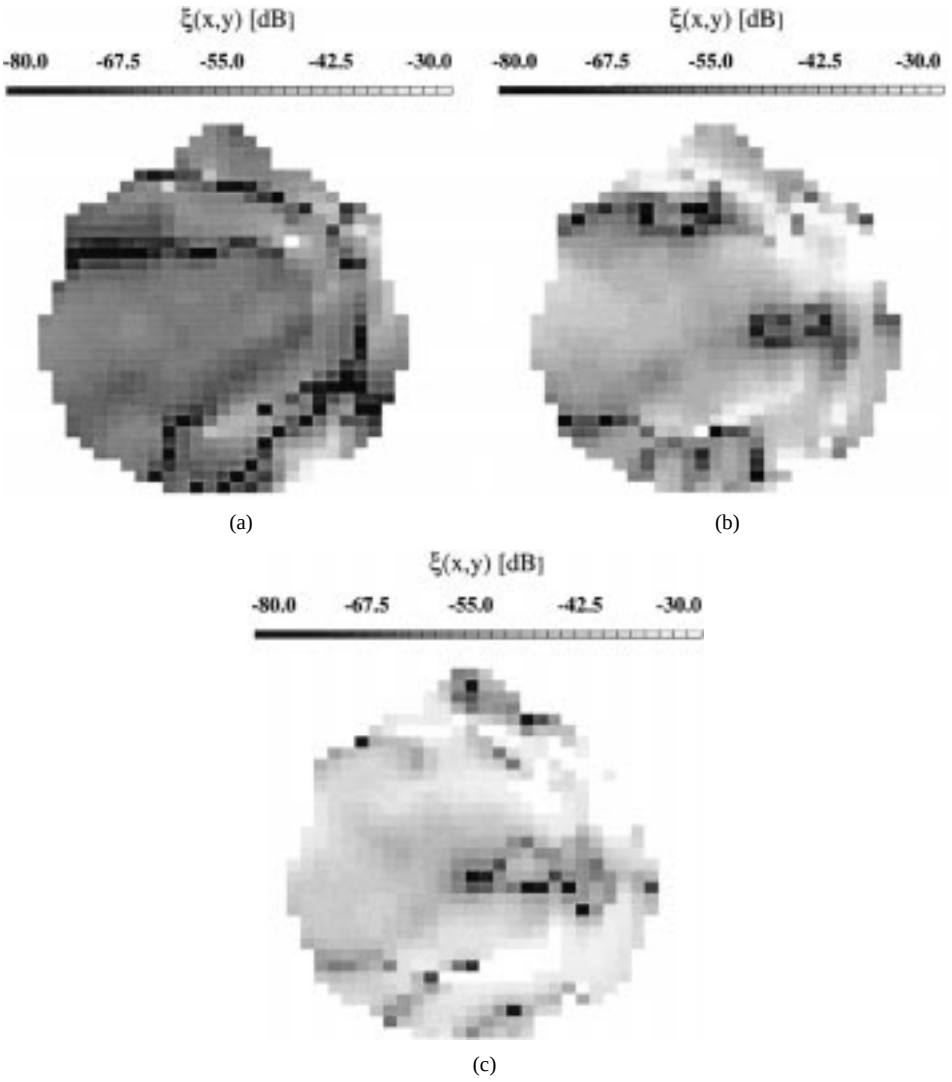

Fig. 8. Error in the estimation of the electric-field amplitude. (a) $t = 0.1$. (b) $t = 0.5$. (c) $t = 1.0$.

For all configurations, the electric field is accurately estimated inside the whole biological structure. The average amplitude error is always lower than -40.8 dB and $\mathrm{av}\{\phi(x, y)\} < 2.84 \cdot 10^{-3}$. Moreover, the amplitude peak is correctly detected and its value well predicted ($\xi(x_p, y_p) \leq -38$ dB) for each value of t.

IV. Conclusions

In this paper, a finite-element procedure, based on a boundary-value approach, for the evaluation of the electromagnetic exposure in biological phantoms has been presented. Starting from the knowledge of the tangential component of the electric field at a number of points around the biological structure, the electric-field distribution has been estimated by solving a suitably defined boundary-value problem. It allows to avoid the characterization of the electromagnetic source and to evaluate the electromagnetic exposure when the illuminating source is completely unknown or when its numerical model is not available.

The effectiveness of the proposed technique has been checked, by considering numerical examples for which analytical reference solutions were available, and further assessed by analyzing a more complicated two-dimensional geometry. It results in a very high accuracy when measurement points are coincident with all boundary nodes. The use of a lower number of measurement points and the accuracy achievable in this case have also been evaluated. Moreover, the effects of noisy measurement data has been taken into account and good results have been obtained for SNRs greater or equal to 20 dB. Finally, the effectiveness of the boundary-value approach to errors in the positioning of the measurement system has been assessed.

References

[1] H. R. Chuang and K. M. Chen, "A numerical method for the computation of induced currents inside 3-D heterogeneous biological bodies by ELF-LF electric fields," *IEEE Trans. Biomed. Eng.*, vol. 36, pp. 628–634, June 1989.

[2] R. G. Olsen, S. L. Backus, and R. D. Steam, "Development and validation of software for predicting ELF magnetic fields near power lines," *IEEE Trans. Power Delivery*, vol. 10, pp. 1525–1534, July 1995.

[3] T. W. Dawson and M. A. Stuchly, "High resolution organ dosimetry for human exposure to low frequency magnetic fields," *IEEE Trans. Magn.*, vol. 34, pp. 1–11, May 1998.

[4] N. C. Skaropoulos, M. P. Ioannidou, and D. P. Chrissoulidis, "Induced EM field in a layered eccentric spheres model of the head: Plane-wave and localized source exposure," *IEEE Trans. Microwave Theory Tech.*, vol. 44, pp. 1963–1973, Oct. 1996.
[5] R. W. P. King, "Electric fields induced in cells in the bodies of amateur radio operators by their transmitting antennas," *IEEE Trans. Microwave Theory Tech.*, vol. 48, pp. 2155–2158, Nov. 2000.
[6] X. K. Kang, L. W. Li, M. S. Leong, and P. S. Kooi, "Specific absorption rate distributions in a multilayered spheroidal human head model exposed to mobile dipoles," *Radio Sci.*, vol. 35, pp. 247–256, 2000.
[7] K. L. Virga and Y. Rahmat-Samii, "Efficient wide-band evaluation of mobile communications antennas using Z or Y matrix interpolation with the method of moment," *IEEE Trans. Antennas Propagat.*, vol. 47, pp. 65–76, Jan. 1999.
[8] K. D. Paulsen, P. M. Meaney, M. J. Moskowitz, and J. M. Sullivan, "A dual mesh scheme for finite element based reconstruction algorithms," *IEEE Trans. Med. Imag.*, vol. 14, pp. 504–514, Sept. 1995.
[9] P. M. Meaney, K. D. Paulsen, and J. T. Chang, "Near-field microwave imaging of biologically based materials using a monopole tranceiver system," *IEEE Trans. Microwave Theory Tech.*, vol. 46, pp. 31–45, Jan. 1998.
[10] M. A. Mangoud, R. A. Abd-Alhameed, and P. S. Excell, "Simulation of human interaction with mobile telephones using hybrid techniques over coupled domains," *IEEE Trans. Microwave Theory Tech.*, vol. 48, pp. 2014–2021, Nov. 2000.
[11] X. Yuan, D. R. Lynch, and J. W. Strohbehn, "Coupling of finite element and moment methods for electromagnetic scattering from inhomogeneous objects," *IEEE Trans. Antennas Propagat.*, vol. 38, pp. 386–393, Mar. 1990.
[12] H. Rogier, D. De Zutter, and F. Olyslager, "Modeling complex structures by combining the FE, FDTD and BIE techniques," in *IEEE AP-S Int. Symp.*, vol. 2, 1999, pp. 1062–1065.
[13] M. A. Jensen and Y. Rahmat-Samii, "EM interaction of handset antennas and a human in personal communications," *Proc. IEEE*, vol. 83, pp. 7–17, Jan. 1995.
[14] L. Martens, J. DeMoerloose, and D. De Zutter, "Calculation of the electromagnetic fields induced in the head of an operator of a cordless telephone," *Radio Sci.*, vol. 30, pp. 283–290, 1995.
[15] M. Okoniewski and M. A. Stuchly, "A study of the handset antenna and human body interaction," *IEEE Trans. Microwave Theory Tech.*, vol. 44, pp. 1855–1864, Oct. 1996.
[16] O. P. Gandhi, G. Lazzi, and C. M. Furse, "Electromagnetic absorption in the human head and neck for mobile telephones at 835 and 1900 MHz," *IEEE Trans. Microwave Theory Tech.*, vol. 44, pp. 1884–1897, Oct. 1996.
[17] P. J. Dimbylow, "FDTD calculation of the whole-body average SAR in an anatomically realistic voxel model of the human body from 1 MHz to 1 GHz," *Phys. Med. Biol.*, vol. 42, pp. 479–490, 1997.
[18] M. Okoniewski and M. A. Stuchly, "Modeling of interaction of electromagnetic field from a cellular telephone with hearing aids," *IEEE Trans. Microwave Theory Tech.*, vol. 46, pp. 1686–1693, Nov. 1998.
[19] J. T. Rowley and R. B. Waterhouse, "Performance of shorted microstrip patch antennas for mobile communications handsets at 1800 MHz," *IEEE Trans. Antennas Propagat.*, vol. 47, pp. 815–822, May 1999.
[20] M. F. Iskander, Z. Yun, and R. Quintero-Illera, "Polarization and human body effects on the microwave absorption in a human head exposed to radiation from handheld devices," *IEEE Trans. Microwave Theory Tech.*, vol. 48, pp. 1979–1987, Nov. 2000.
[21] K. Caputa, M. A. Stuchly, M. Skopec, H. I. Bassen, P. Ruggera, and M. Kanda, "Evaluation of electromagnetic interference from a cellular telephone with a hearing aid," *IEEE Trans. Microwave Theory Tech.*, vol. 48, pp. 2148–2154, Nov. 2000.
[22] W. R. Stone, Ed., *Review of Radio Science 1996–1999*. Oxford, U.K.: Oxford Sci..
[23] S. Caorsi and A. Massa, "A microwave-imaging technique for electromagnetic exposure prediction: Preliminary results," *Microwave Opt. Technol. Lett.*, vol. 19, pp. 328–332, 1998.
[24] ——, "Electromagnetic field prediction inside biological bodies by using an inverse scattering procedure based on a statistical cooling algorithm," *Bioelectromagnetics*, vol. 21, pp. 422–431, 2000.
[25] S. Caorsi, E. Bermani, and A. Massa, "A microwave imaging approach based on amplitude-only data for the reconstruction of the electromagnetic field induced in biological phantoms," *Appl. Comput. Electromagn. Soc. J. (Special Issue)*, vol. 16, pp. 79–89, 2001.
[26] C. A. Balanis, *Advanced Engineering Electromagnetics*. New York: Wiley, 1989.
[27] J. Jin, *The Finite Element Method in Electromagnetics*. New York: Wiley, 1993.
[28] M. R. Hestenes and E. Stiefel, "Method of conjugate gradients for solving linear systems," *J. Res. Natl. Bur. Stand.*, vol. 49, pp. 409–436, 1952.
[29] H. Whitney, *Geometric Integration Theory*. Princeton, NJ: Princeton Univ. Press, 1957.
[30] Z. S. Sacks, D. M. Kingsland, R. Lee, and J.-F. Lee, "A perfectly matched anisotropic absorber for use as an absorbing boundary condition," *IEEE Trans. Antennas Propagat.*, vol. 43, pp. 1460–1463, Dec. 1995.
[31] A. Franchois, A. Joisel, C. Pichot, and J. C. Bolomey, "Quantitative microwave imaging with a 2.45-GHz planar microwave camera," *IEEE Trans. Med. Imag.*, vol. 17, pp. 550–561, Aug. 1998.

Salvatore Caorsi (M'98) received the Laurea degree in electronic engineering from the University of Genoa, Genoa, Italy, in 1973.

Upon graduation, he remained with the University of Genoa as a Researcher and, since 1976, he has been a Professor of antennas and propagation. In 1985, he also became a Professor of fundamentals of remote sensing. Since 1994, he has been a Full Professor of electromagnetic compatibility with the Department of Electronics, University of Pavia, Pavia, Italy. He is the past Chairman of the Inter-university Research Center for Interactions Between Electromagnetic Fields and Biological Systems (ICEMB). His primary activities are focused on applications of electromagnetic fields to telecommunications, artificial vision and remote sensing, biology, and medicine. In particular, he is currently involved with research projects concerning microwave hyperthermia and radiometry in oncological therapy, numerical methods for solving electromagnetic problems, and inverse scattering and microwave imaging.

Dr. Caorsi is a member of the Associazione Elettrotecnica ed Elettronica Italiana (AEI), the European Bioelectromagnetism Association (EBEA), and the European Society for Hyperthermic Oncology (ESHO).

Emanuela Bermani received the Laurea degree in electronic engineering and Ph.D. degree in electronics and computer science from the University of Pavia, Pavia, Italy, in 1997 and 2000, respectively.

She is currently an Assistant Professor with the University of Trento, Trento, Italy. Her research interests are mainly focused on electromagnetic direct and inverse scattering, bioelectromagnetics, and theoretical electromagnetics.

Andrea Massa (M'01) received the Laurea degree in electronic engineering and Ph.D. degree in electronics and computer science from the University of Genoa, Genoa, Italy, in 1992 and 1996, respectively.

From 1997 to 1999, he was an Assistant Professor of electromagnetic fields with the Department of Biophysical and Electronic Engineering, University of Genoa, where he taught "Electromagnetic Fields 1." He is currently an Associate Professor with the University of Trento, Trento, Italy, where he teaches "Electromagnetic Fields" and "Electromagnetic Diagnostic Techniques." He is a member of the Inter-university Research Center for Interactions Between Electromagnetic Fields and Biological Systems (ICEmB). Since 1992, his research has principally concerned electromagnetic direct and inverse scattering, optimization techniques for microwave imaging, wave propagation in the presence of nonlinear media, applications of electromagnetic fields to telecommunications, medicine, and biology.